View metadata, citation and similar papers at core.ac.uk

brought to you by CORE

provided by Purdue E-Pubs

Purdue University
Purdue e-Pubs

Department of Electrical and Computer Engineering Faculty Publications

Department of Electrical and Computer Engineering

1993

Concentration-dependent optical-absorption coefficient in n-type GaAs

Gregory Benedict Lush
Purdue University

H. F. MacMillan
Varian Research Center, Palo Alto, CA

S. Asher
National Renewable Energy Laboratory, Golden, Colorado

Michael R. Melloch
Purdue University, melloch@purdue.edu

Mark S. Lundstrom
Purdue University, lundstro@purdue.edu

Follow this and additional works at: https://docs.lib.purdue.edu/ecepubs

Part of the Electrical and Computer Engineering Commons

Lush, Gregory Benedict; MacMillan, H. F.; Asher, S.; Melloch, Michael R.; and Lundstrom, Mark S., "Concentration-dependent optical-absorption coefficient in n-type GaAs" (1993). *Department of Electrical and Computer Engineering Faculty Publications.* Paper 98.
https://docs.lib.purdue.edu/ecepubs/98

This document has been made available through Purdue e-Pubs, a service of the Purdue University Libraries. Please contact epubs@purdue.edu for additional information.

.

Concentration-dependent optical-absorption coefficient in n-type GaAs

G. B. Lush, M. R. Melloch, and M. S. LundstromH. F. MacMillanS. Asher

Citation: **74**, (1993); doi: 10.1063/1.354336
View online: http://dx.doi.org/10.1063/1.354336
View Table of Contents: http://aip.scitation.org/toc/jap/74/7
Published by the American Institute of Physics

RIGHTSLINK
Copyright Clearance Center

Concentration-dependent optical-absorption coefficient in *n*-type GaAs

G. B. Lush, M. R. Melloch, and M. S. Lundstrom
School of Electrical Engineering, Purdue University, W. Lafayette, Indiana 47907

H. F. MacMillan
Varian Research Center, Palo Alto, California 94303

S. Asher
National Renewable Energy Laboratory, Golden, Colorado 80401

(Received 27 April 1992; accepted for publication 15 June 1993)

The doping-dependent, near-band-edge optical-absorption coefficient $\alpha(h\nu)$ was deduced from optical transmission measurements in *n*-type GaAs thin films. The selenium-doped films were grown by metalorganic chemical-vapor deposition and doped to produce room-temperature electron concentrations from 1.3×10^{17} to 3.8×10^{18} cm^{-3}. The transmission measurements covered photon energies between 1.35 and 1.7 eV and were performed on double heterostructures with the substrate removed by selective etching. The results show good qualitative agreement with previous studies and good quantitative agreement, except for the heavily doped samples. For $n_0=3.8\times10^{18}$ cm^{-3}, $\alpha(1.42$ eV$)$ is approximately four times that reported by previous workers. Secondary-ion-mass spectrometry measurements on films grown under differing conditions demonstrate that $\alpha(h\nu)$ is sensitive to electrically inactive dopants and supports the hypothesis that precipitates or compensation influenced previous measurements. These comprehensive results on high-quality, uncompensated material should prove useful for fundamental studies of optical transitions in *n*-type GaAs as well as for modeling optoelectronic devices.

I. INTRODUCTION

Knowledge of the doping dependence of the near-band-edge absorption coefficient versus photon energy $\alpha(h\nu)$ is vital to describe photoluminescence in GaAs,[1–3] to calculate the emission spectra for GaAs lasers,[4] to model photon recycling in double heterostructures,[5–8] and to test band-structure calculations of heavily doped GaAs.[9–11] Workers in these fields typically make use of the classic and comprehensive study of $\alpha(h\nu)$ by Casey, Sell, and Wecht,[12] but in a later paper, Casey and Stern[4] expressed concern about the data for *n*-type GaAs. Their concern stemmed from the fact that they were unable to model theoretically the measured $\alpha(h\nu)$, its use in the van Roosbroeck–Shockley expression[13] did not produce the measured emission spectra,[4] and because the results differed from those of previous efforts.[2,14] Because the measurements of Casey and co-workers were performed on melt-grown GaAs, there was concern that compensation and precipitates might have influenced the results.[4] In spite of these concerns, workers have continued to use the data of Casey and co-workers because there are no other comprehensive data available.

In this article we present a comprehensive characterization of the doping-dependent, near-band-edge absorption coefficient in *n*-type GaAs grown by modern epitaxial techniques. Transmission experiments were used to deduce $\alpha(h\nu)$ over the photon energy range of 1.35–1.7 eV. The six selenium-doped films had room-temperature electron concentrations from 1.3×10^{17} to 3.8×10^{18} cm^{-3} and were grown by metalorganic chemical-vapor deposition (MOCVD). While the qualitative agreement with Casey and co-workers' work is good, we find important quantitative differences. For electron concentrations less than 10^{18} cm^{-3}, we find good agreement with Casey and co-workers' data for the absorption tail, but for higher energies we find that α is 20%–25% larger than is Casey and co-workers'. At the highest electron concentration studied, we find that $\alpha(1.42$ eV$)$ for our samples is four times higher than that measured by Casey and co-workers. We demonstrate that Casey and co-workers' measurements were likely influenced by compensation in his samples. This new and comprehensive data for high-quality, *n*-type GaAs will prove useful for basic studies as well as for device modeling.

II. EXPERIMENTAL PROCEDURES

The *n*-GaAs films were double heterostructures (DHs) grown by MOCVD at atmospheric pressure on horizontal-Bridgman substrates heated to 740 °C by radio-frequency induction. The growth rate was 6 μm/h, except for the films with $n_0=2.4\times10^{18}$ cm^{-3} for which the growth rate was 4 μm/h. The doping agent was hydrogen selenide (from Scott Specialty Gases) diluted to 55 ppm with hydrogen, and the sources were trimethyl aluminum, trimethyl gallium, and 100% arsine. The V/III ratio was maintained at 30, with the exception of the films with $n_0=2.4\times10^{18}$ cm^{-3} for which the V/III ratio was 45. Further details of the growth are described elsewhere.[15]

The basic structure of the DHs is shown in Fig. 1. The cladding $Al_{0.3}Ga_{0.7}As$ layers provide carrier confinement for lifetime measurements[15] while the $Al_{0.85}Ga_{0.15}As$ acts as an etch-stop layer.[16] The electron concentrations tabulated in Table I were measured by the van der Pauw technique using the thickest film at each concentration. The selenium concentration was measured by secondary-ion-

 0021-8979/93/74(7)/4694/9/$6.00 © 1993 American Institute of Physics

RIGHTSLINK

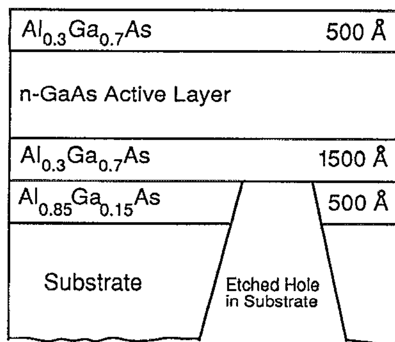

FIG. 1. The basic structure of the double heterostructures grown for this study. The $Al_{0.85}Ga_{0.15}As$ layer acts as an etch stop.

mass spectrometry (SIMS) in a Cameca IMS-3f using cesium as the ionizing source. The electron concentration was found to be approximately equal to the selenium concentration for all films except those grown at 4 μm/h ($n_0=2.4\times10^{18}$ cm^{-3}). Table I lists the measured thickness of each of the DHs used in this study. The thicknesses were determined with a scanning electron microscope (SEM) by viewing an adjacent piece of the wafer after it had been "stained" by a 25 s dip in a solution of de-ionized (DI) water, hydrofluoric acid (HF), and 30% hydrogen peroxide (H_2O_2) mixed with a ratio of 10:1:1 DI:HF:H_2O_2.

To prepare the samples for the transmission experiments, a hole was etched through the substrate by wet chemical etching. The samples were placed face down in black wax melted on a glass slide. The wax covered the edges and part of the substrate, leaving an area of the substrate exposed in the middle. The mounted sample was then immersed in a room-temperature solution of 50 g of granular citric acid dissolved in 50 ml of DI water and 10 ml of H_2O_2. The typical etching time before the $Al_{0.85}Ga_{0.15}As$ layer was exposed was 36 h. Since this mixture etches $Al_{0.85}Ga_{0.15}As$ as much as 100 times more slowly than it etches GaAs,[16,18] the area of exposed $Al_{0.85}Ga_{0.15}As$ looked specular relative to the rough back of the substrate. Once this specular area of exposed $Al_{0.85}Ga_{0.15}As$ was large enough (2–3 mm in diameter), the sample was rinsed in DI and the $Al_{0.85}Ga_{0.15}As$ layer was removed by a 30 s dip in hydrogen fluoride (HF) diluted with DI to 5% by volume. (HF removes high mole fraction AlGaAs much faster than it does low mole fraction AlGaAs.[17,19]) The sample was then unmounted by soaking in trichloroethane. The thin film was still attached at the periphery to the substrate, so the sample was easily handled with tweezers. Where the substrate was removed, the thinner DHs ($w<4$ μm) exhibited a slight bowing possibly due to the lattice mismatch of the GaAs-AlGaAs interfaces, but no evidence of strain was observed in the results.

TABLE I. Measured GaAs electron densities and thicknesses for each of the double heterostructures used for this study.

n_0 (cm^{-3})		Measured thicknesses (μm)	
1.3×10^{17}	2.2	4.68	8.6
3.7×10^{17}	2.32	5.55	9.67
1.0×10^{18}	1.65	3.5	5.8
2.2×10^{18}	2.6	4.55	9.0
2.4×10^{18}	···	2.25	9.15
3.8×10^{18}	···	2.12	8.7

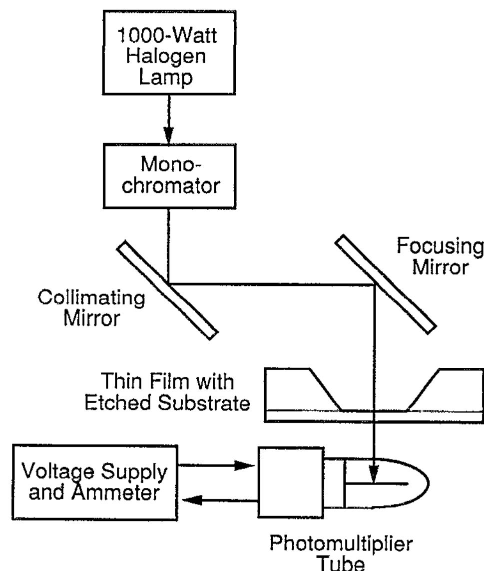

FIG. 2. Block diagram of the experimental setup.

Figure 2 shows a block diagram of the experimental apparatus. The output of a 1000 W halogen lamp was focused onto the input slit of a $\frac{1}{8}$ m scanning monochromator. The slit widths were set to 0.3 mm which allowed a bandpass of less than 2 nm full width at half-maximum at 545 nm. (This was measured by observing the output of the monochromator illuminated with a mercury vapor lamp.) A long-pass filter with a 50% cutoff at $\lambda=630$ nm was used to block higher-order wavelengths transmitted through the monochromator. The output of the monochromator was collimated using a fused silica plano convex lens and an aluminum mirror with a radius of curvature of 1.0 m. The focusing mirror had a 0.1 m radius of curvature, narrowing the light beam to an area about 2 mm in diameter. Light detection was by an S1 photomultiplier used at room temperature. The measurements were taken while the room temperature was 18–20 °C. The output wavelength of the monochromator was varied from 700 to 1000 nm in steps of 2.0 nm. Data were taken over all wavelengths with the sample illuminated from the back side, and then data were recorded with the sample removed.

III. DEDUCING ABSORPTION COEFFICIENT FROM TRANSMITTANCE

This section describes the general technique we use to analyze the transmittance data, and then as an aid to understanding we detail the analysis for the samples with $n_0=3.7\times10^{17}$ cm^{-3}. The transmittance $T(h\nu)$, or fraction

RIGHTSLINK

of light transmitted through a three-layer absorbing structure, is a complicated function of the complex indices of refraction and thicknesses of the three layers.[20,21] For strongly absorbed light, interference effects are minimal, which greatly simplifies the expression for $T(h\nu)$. Additional simplifications result because there is no absorption in the $Al_{0.3}Ga_{0.7}As$ cladding layers for the wavelength range of interest, and because the reflectivity at the $Al_{0.3}Ga_{0.7}As$-GaAs interfaces is less than 1%.[22–24] Sell and Casey used these simplifications to write the transmittance of a three-layer $Al_xGa_{1-x}As/GaAs/Al_xGa_{1-x}As$ structure as[25]

$$T(h\nu)=\frac{(1-R)^2e^{-\alpha(h\nu)w}}{1-R^2e^{-2\alpha(h\nu)w}}. \quad (1)$$

For our work, R is the reflectance of a single air-$Al_{0.3}Ga_{0.7}As$ interface (not the reflectance of the three-layer structure), and w is the thickness of the GaAs active layer. Equation (1) ignores interference effects, which only affect measurements with weakly absorbed light. In Eq. (1) both $T(h\nu)$ and w are determined experimentally so only R is needed to deduce $\alpha(h\nu)$.

For very low-energy photons the DHs are nonabsorbing Fabry–Perot cavities; the well-known relationship between the transmittance of a Fabry–Perot cavity and R is written as[26]

$$T'(h\nu)=\frac{(1-R)^2}{(1-R)^2+4R\sin^2\Theta}, \quad (2)$$

where $\Theta=2\pi w n_{\text{eff}}/\lambda$, and n_{eff} is the index of refraction. Equation (2) shows that there is no unique value of $T'(h\nu)$ from which we can deduce a value for R. We can, however, define a quantity T_{ave}, which is the average of $T'(h\nu)$ for photons below the band gap. $T'(h\nu)$ in Eq. (2) peaks in intervals of $\Theta=m\pi$, where m is an integer, so to find T_{ave} theoretically one integrates Eq. (2) for one period between $\Theta=m\pi$ and $\Theta=(m+1)\pi$ [two arbitrary peaks in $T'(h\nu)$] and divides by the length of the integrand π (this is detailed in the Appendix). The result of this integration[27] is that

$$T_{\text{ave}}=\frac{1-R}{1+R}, \quad (3)$$

which directly relates T_{ave} and R. T_{ave} can be computed from experiment by averaging the $T(h\nu)$ data over the range of photon wavelengths where $0.9<\lambda<1.0$ μm and $\alpha(h\nu)=0$. For all electron concentrations, T_{ave} of the thickest DH was within ± 0.01 of 0.54. Equation (3) yields $R=0.30\pm 0.01$ and Eq. (4) below gives values of 3.4 ± 0.1 for the index of refraction of the $Al_{0.3}Ga_{0.7}As$ layers. Previous authors[22,23] obtained $n\simeq 3.4$ in nominally undoped $Al_{0.3}Ga_{0.7}As$ for this range of photon energies.

An issue which arises in using Eq. (1) to relate $T(h\nu)$ and $\alpha(h\nu)$ is that Eq. (1) assumes that R is independent of energy. To demonstrate that this generates little uncertainty, we can compute R by

$$R=\left(\frac{n-1}{n+1}\right)^2, \quad (4)$$

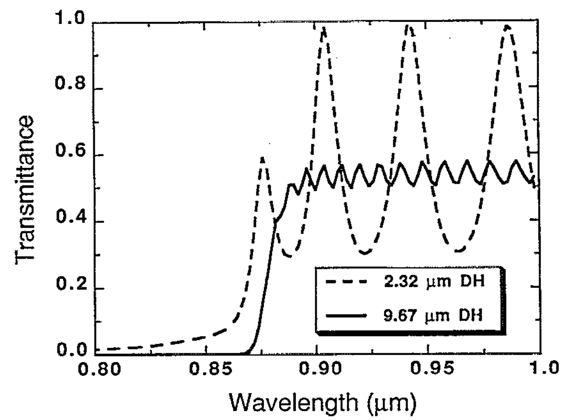

FIG. 3. Transmittance vs photon wavelength for two DHs with $n_0=3.7\times 10^{17}$ cm^{-3}. The oscillations for photon energies below the band-gap energy are due to interference effects which one can model by treating the DH as a Fabry–Perot cavity.

where data for n, the index of refraction of the nonabsorbing $Al_{0.3}Ga_{0.7}As$ layers, are taken from the literature for nominally undoped $Al_{0.3}Ga_{0.7}As$.[23] We find that $R=0.31\pm 0.01$ for the photon energies of interest, which is similar to that deduced from T_{ave}. The reason we deduce R from T_{ave} rather than from the literature data for n of the $Al_{0.3}Ga_{0.7}As$ is that our $Al_{0.3}Ga_{0.7}As$ layers are highly doped and the literature data are for nominally undoped $Al_{0.3}Ga_{0.7}As$.[23]

Using Eq. (1), we have the greatest confidence in the $\alpha(h\nu)$ deduced from the measured transmittance for $0.005<T(h\nu)<0.35$. $T(h\nu)\simeq 0.005$ is the limit of our experimental accuracy, and for $T(h\nu)>0.35$, multiple internal reflections can cause increased uncertainty. Figure 3 shows the transmittance for two of the DHs with $n_0=3.7\times 10^{17}$ cm^{-3}. The oscillations for photon energies below the band-gap energy are due to interference effects which one can model by treating the DH as a Fabry–Perot cavity. The transmittance of the sample with $w=2.32$ μm peaks near 1.0, which indicates that the surfaces are specular. By noting the regions of the plots of Fig. 3 where $0.005<T(h\nu)<0.35$, it is observed that each of the two DHs has a different wavelength range for which $\alpha(h\nu)$ can be deduced. Each DH thickness, therefore, contributes to a different region of the final plot of $\alpha(h\nu)$. Overlap between two regions provides a check for self-consistency. An illustration of this is shown in Fig. 4 which plots the contribution from each of the three DHs used to deduce $\alpha(h\nu)$ for $n_0=3.7\times 10^{17}$ cm^{-3}. The broken and solid lines delineate the contributions of each DH to the deduced $\alpha(h\nu)$.

The low-energy region of the curve shows how the interference effects seen in Fig. 3 can generate oscillations in the results if $T(h\nu)>0.35$. [Only for the thickest DH at each electron concentration were data for $T(h\nu)>0.35$ used.] The phase of a photon is highly sensitive to the index of refraction and thickness of each layer; we could not model the phase for our structures, because we do not know the precise thicknesses of the $Al_{0.3}Ga_{0.7}As$ layers and because there are no data for the index of refraction for

RIGHTSLINK

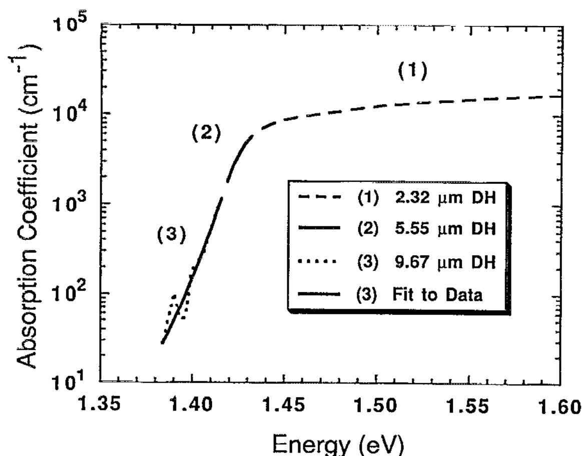

FIG. 4. Plot showing how each double-heterostructure thickness [regions (1)–(3)] contributes to determining $\alpha(h\nu)$ for $n_0=3.7\times10^{17}$ cm^{-3}. The region of the curve with smallest $\alpha(h\nu)$ also shows how the interference effects seen in Fig. 3 can generate oscillations in the results. The line drawn through the oscillations is the result of a least-squares fit to the log of $\alpha(h\nu)$. This was done for all doping concentrations in a like manner to produce the final results.

heavily doped $Al_{0.3}Ga_{0.7}As$. We therefore "draw" a line through the oscillations by performing a least-squares fit to the log of $\alpha(h\nu)$ deduced from the $T(h\nu)$ data of that particular DH. This was done for all electron concentrations in a like manner to produce the final results. Interestingly, we found that the magnitude of the Fabry–Perot-like oscillations in $T(h\nu)$ increased with increasing selenium concentration, making it increasingly difficult to deduce $\alpha(h\nu)$ for weakly absorbed light. Figure 5 illustrates this by showing $\alpha(h\nu)$ deduced from Eq. (1) for the 8.7 μm DH with $n_0=3.8\times10^{18}$ cm^{-3} and also shows the least-squares fit for $\alpha(h\nu)$ of that DH. Although the oscillations are much stronger than those depicted in Fig. 4, the least-squares fit describes the data nicely.

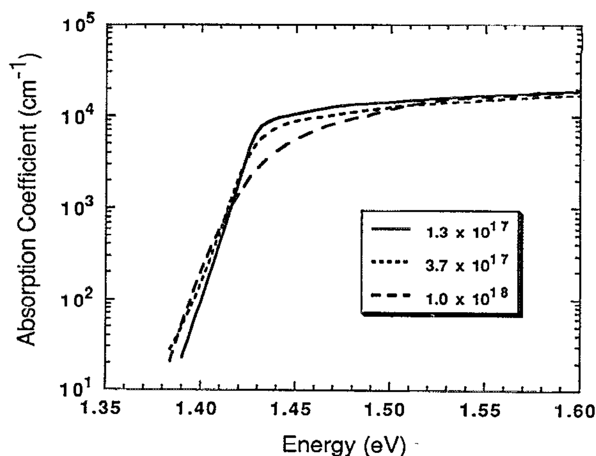

FIG. 6. Room-temperature results of $\alpha(h\nu)$ for $n_0 \leqslant 1.0\times10^{18}$ cm^{-3}.

IV. RESULTS

Figures 6 and 7 show the results for the six electron concentrations. For $n_0 \leqslant 1.0\times10^{18}$ cm^{-3}, the data displayed in Fig. 6 show behavior that is qualitatively similar to that of previous authors.[2,12,14] The data show the expected exponential absorption tail known as the Urbach tail.[28] Blakemore[29] has reviewed possible causes of the Urbach tail seen in previous studies. In accordance with previous concentration-dependent works,[2,12,14] the slope of the absorption tails in Figs. 6 and 7 is observed to decrease with increasing electron concentration; this effect is typically attributed to tails in the density of states, caused by the impurity atoms.[4,30] As n_0 increases, the absorption tail is shifted to higher energies, which is due to the filling of electron states, known as the Burstein shift.[31] Of special note is the fact that the value of $\alpha(h\nu)$ at $h\nu=1.7$ eV for $n_0=3.7\times10^{17}$ cm^{-3} is about 9% below the corresponding values for the concentrations of $n_0=1.3\times10^{17}$ cm^{-3} and

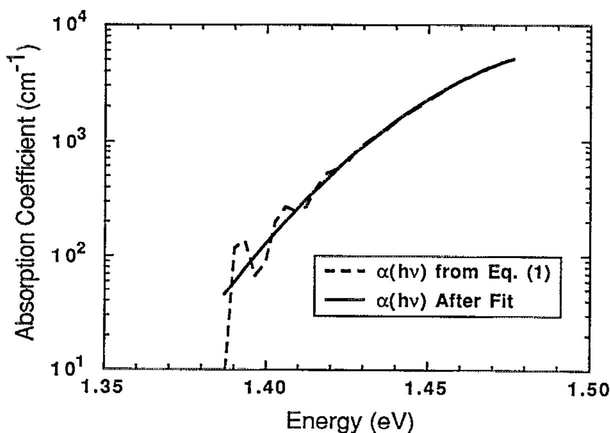

FIG. 5. Plot comparing $\alpha(h\nu)$ before and after least-squares fit to the data deduced from Eq. (1) for the 8.7 μm DH with $n_0=3.8\times10^{18}$ cm^{-3}.

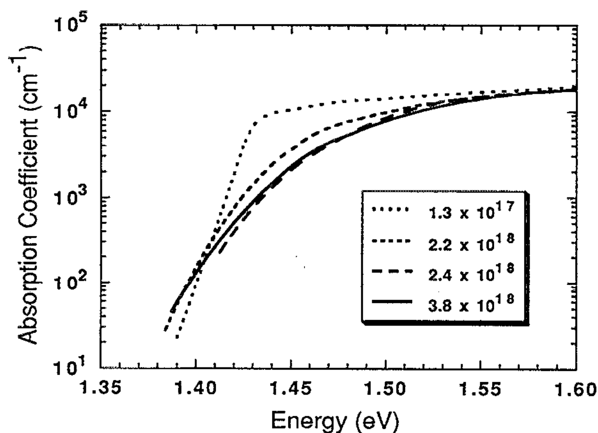

FIG. 7. Room-temperature results of $\alpha(h\nu)$ for $n_0 \geqslant 2.2\times10^{18}$ cm^{-3}. Also shown is $\alpha(h\nu)$ for $n_0=1.3\times10^{17}$ cm^{-3} for reference.

RIGHTSLINK

$n_0=1.0\times10^{18}$ cm^{-3} (see Table II). A similar effect was also observed by Casey and co-workers for $n_0=5.9\times10^{17}$ cm^{-3}.

As shown in Fig. 7, the slope of the absorption tail continues to decrease with increasing electron concentration for $n_0>10^{18}$ cm^{-3}, and the magnitude of the Burstein shift continues to increase. At high energies $\alpha(h\nu)$ approaches nearly the same value for those four electron concentrations depicted in Fig. 7, and with the exception of $n_0=3.7\times10^{17}$ cm^{-3}, the values of $\alpha(h\nu)$ at $h\nu=1.7$ eV for all concentrations are within $2.32\pm0.07\times10^4$ cm^{-1}. Table II lists the values of $\alpha(h\nu)$ for five of the six electron concentrations; the data for $n_0=2.4\times10^{18}$ cm^{-3}, omitted because they are inconsistent with the others, are discussed in Sec. V.

A significant aspect of these results is that $\alpha(h\nu)$ for $n_0=2.2\times10^{18}$ cm^{-3} and $n_0=2.4\times10^{18}$ cm^{-3} are quite dissimilar while $\alpha(h\nu)$ of 2.4 and 3.8×10^{18} cm^{-3} are nearly indistinguishable. Remember that the films with $n_0=2.4\times10^{18}$ cm^{-3} were grown at a slower rate by adjusting the III-V flow ratio. In Sec. V we discuss results of SIMS measurements which show that the actual concentration of selenium in the films with the electron concentration of $n_0=2.4\times10^{18}$ cm^{-3} was $N_{Se}=4.1\times10^{18}$ atoms/cm^3, far greater than the free-electron concentration given by the van der Pauw technique.

Uncertainty in the results for extracted $\alpha(h\nu)$ arises largely from uncertainty in $T(h\nu)$, R, w, and the interference effects. Measured values for $T(h\nu)$ and w should be accurate to within 1%, and Sec. III showed that R is accurate to within about 3%—which leads to $\simeq$3% uncertainty in the quantity $(1-R)^2$. This means that the expected uncertainty of $\alpha(h\nu)$ deduced from data within the range for which $0.005 < T(h\nu) \leq 0.35$ is about 3%, and this is consistent with the results for $h\nu=1.7$ eV.

V. DISCUSSION

We now quantitatively compare our results to the often-cited data reported by Casey and co-workers,[12] which is the most comprehensive study of $\alpha(h\nu)$ in n-type GaAs. Casey and co-workers combined transmission measurements on thick samples to determine $\alpha(h\nu)$ for values less than 10^3 cm^{-1} and a Kramers–Kroenig[32] analysis of reflection measurements to determine higher $\alpha(h\nu)$. Since the carrier concentrations of our samples differ from those of Casey and co-workers, the "results" we present from their work are actually interpolated to the electron concentrations we measured in our samples. Also, Casey and co-workers did not measure the absorption tail of their sample with $n_0=5.0\times10^{16}$ cm^{-3}, but instead used Sturge's data[33] to complete the plot. Finally, to quantitatively compare the results in the absorption edge, one must first account for the expected change in the band gap due to differences in the measurement temperatures [about 0.5 meV/K near our measurement temperature of $T\simeq292$ K (Ref. 29)]. Casey and co-workers' data, measured at $T=297$ K and shown in Figs. 8 and 9, do not include the $\simeq$2.5 meV shift because it is not observable for the scale used in those figures.

For our $n_0=1.3\times10^{17}$ cm^{-3} samples, we find a steeper absorption tail than did Casey and co-workers, but a slope similar to that of Sturge. Our $\alpha(h\nu)$ above the band gap are larger than the data of Casey and co-workers by about 20%–25%. For $n_0=3.7\times10^{17}$ and 1.0×10^{18} cm^{-3}, our results agree with those of Casey and co-workers for $\alpha(h\nu)$ <3000 cm^{-1}, as represented in Fig. 8 for $n_0=3.7\times10^{17}$ cm^{-3}; but, again, our $\alpha(h\nu)$ above the band gap are larger than the data of Casey and co-workers. Thus, we do find strong quantitative agreement with Casey and co-workers, but only in a narrow range of electron concentration and only in the region where they relied on transmission experiments for deducing $\alpha(h\nu)$. Casey and Stern felt that the Kramers–Kroenig analysis would be less accurate on n-type GaAs than on p-type GaAs,[4] so the discrepancy for high-energy photons is not surprising.

At higher electron concentrations, we find that our data differ substantially from those of Casey and co-workers for $n_0=2.2$ and 3.8×10^{18} cm^{-3}, but are similar in the absorption edge for $n_0=2.4\times10^{18}$ cm^{-3}. Figure 9 compares our results for $n_0=3.8\times10^{18}$ cm^{-3} to those of Casey and co-workers interpolated to $n_0=2.4$ and 3.8×10^{18} cm^{-3}. For $n_0=3.8\times10^{18}$ cm^{-3}, our data show a steeper Urbach tail and the absorption edge occurs at a lower photon energy, as evidenced by the fact that $\alpha=1000$ cm^{-1} at $h\nu=1.43$ eV for our data and at $h\nu\simeq1.47$ eV for that of Casey and co-workers, after the band-gap shift. The ratio of α for $h\nu=1.42$ eV of this work to Casey and co-workers at $n_0=3.8\times10^{18}$ cm^{-3} after the band-gap shift is about four. Although our results for $n_0=3.8\times10^{18}$ cm^{-3} do not agree with Casey and co-workers' for $n_0=3.8\times10^{18}$ cm^{-3}, our results for $n_0=3.8\times10^{18}$ cm^{-3} agree quite well with their $\alpha(h\nu)$ for $n_0=2.4\times10^{18}$ cm^{-3}. Remembering that our $\alpha(h\nu)$ for $n_0=2.4\times10^{18}$ and 3.8×10^{18} cm^{-3} are quantitatively similar, we conclude that our $\alpha(h\nu)$ for $n_0=2.4\times10^{18}$ cm^{-3} agree reasonably well with Casey and co-workers' interpolated data. We discuss below the fact that our films with $n_0=2.4$ and 3.8×10^{18} cm^{-3} and their wafers with n_0 interpolated to $n_0=2.4\times10^{18}$ cm^{-3} all have similar dopant or impurity concentrations although varying electron concentrations. We conclude that it is the similarity of the impurity concentrations that leads to the similarity in $\alpha(h\nu)$ among the three samples with data plotted in Fig. 9.

Figure 10 shows the SIMS data for our films grown by MOCVD. Each sample was probed in several different areas and the measured dopant concentrations averaged to determine the selenium concentration in each sample. The data that were averaged for each sample were within $\pm15\%$ of each other in all cases and within $\pm10\%$ for all but the sample with $n_0=2.2\times10^{18}$ cm^{-3}. Since SIMS is more accurate when trying to find relative concentrations rather than absolute concentrations, the SIMS results were then scaled using the lowest electron concentration measured by the van der Pauw technique to produce the data points in Fig. 10. The abscissa of Fig. 10 is the electron concentration as measured by the van der Pauw technique, the ordinate is the selenium concentration as measured by SIMS, and the line represents the expected electron con-

RIGHTSLINK

TABLE II. Absorption coefficient vs electron concentration and photon energy or wavelength.

λ (μm)	Energy (eV)	Absorption coefficient vs electron concentration				
		1.3×10^{17} (cm^{-1})	3.7×10^{17} (cm^{-1})	1.0×10^{18} (cm^{-1})	2.2×10^{18} (cm^{-1})	3.8×10^{18} (cm^{-1})
0.896	1.384	···	27.6	20.9	27.9	···
0.894	1.387	···	37.0	33.8	39.6	45.5
0.892	1.390	22.8	50.5	53.8	55.5	59.2
0.890	1.393	35.7	70.2	83.7	77.2	76.7
0.888	1.396	56.2	99.4	127.4	106.0	98.4
0.886	1.400	88.9	143.4	189.8	143.9	125.6
0.884	1.403	141.4	210.5	276.3	192.9	159.2
0.882	1.406	226.8	315.4	394.6	256.1	200.7
0.880	1.409	365.1	480.8	549.8	335.8	251.1
0.878	1.412	591.6	747.5	750.7	435.2	312.0
0.876	1.416	965.0	1 185.1	1 002.3	557.9	385.4
0.874	1.419	1 579.8	1 814.3	1 306.8	705.7	472.4
0.872	1.422	2 607.5	2 785.9	1 667.9	883.2	575.1
0.870	1.425	4 326.1	3 742.1	2 080.2	1 091.7	695.9
0.868	1.429	6 257.9	4 798.6	2 534.0	1 332.8	835.8
0.866	1.432	7 788.4	5 729.0	3 019.8	1 608.0	997.2
0.864	1.435	8 650.6	6 492.4	3 514.8	1 917.4	1 181.0
0.862	1.439	9 266.1	7 210.4	3 993.2	2 256.9	1 388.6
0.860	1.442	9 736.3	7 847.3	4 433.3	2 623.9	1 621.7
0.858	1.445	10 020.6	8 303.2	4 916.6	3 013.0	1 880.1
0.856	1.449	10 333.0	8 653.6	5 303.1	3 467.4	2 163.7
0.854	1.452	10 658.9	9 042.8	5 781.7	3 926.2	2 472.1
0.852	1.455	11 020.6	9 300.4	6 285.6	4 461.2	2 805.4
0.850	1.459	11 413.9	9 574.6	6 762.2	5 030.4	3 158.7
0.848	1.462	11 745.1	9 764.8	7 298.4	5 539.7	3 528.6
0.846	1.466	12 102.5	9 981.5	7 790.1	6 083.6	3 915.4
0.844	1.469	12 490.6	10 200.3	8 198.8	6 494.4	4 310.4
0.842	1.473	12 774.2	10 431.0	8 675.9	6 902.1	4 710.8
0.840	1.476	12 930.8	10 685.2	9 013.8	7 298.5	5 050.1
0.838	1.480	13 227.2	10 944.2	9 397.2	7 643.6	5 391.2
0.836	1.483	13 400.7	11 219.9	9 804.8	8 053.3	5 800.0
0.834	1.487	13 581.0	11 527.3	10 042.0	8 383.0	6 225.7
0.832	1.490	13 768.8	11 696.1	10 476.2	8 756.3	6 656.4
0.830	1.494	13 807.2	12 026.7	10 951.9	9 209.2	7 105.0
0.828	1.498	14 004.8	12 216.8	11 468.9	9 584.9	7 562.4
0.826	1.501	14 211.4	12 591.7	11 947.8	9 837.9	8 022.3
0.824	1.505	14 427.8	12 809.3	12 449.8	10 337.8	8 490.9
0.822	1.509	14 655.1	13 038.5	12 895.7	10 790.5	8 966.8
0.820	1.512	14 919.0	13 074.8	13 366.6	11 288.6	9 453.4
0.818	1.516	14 943.7	13 318.9	13 771.6	11 655.1	9 927.2
0.816	1.520	15 225.4	13 557.3	14 181.0	12 078.8	10 413.0
0.814	1.523	18 469.7	13 619.0	14 487.5	12 513.1	10 898.2
0.812	1.527	15 757.4	13 875.1	14 810.4	12 794.8	11 367.5
0.810	1.531	15 817.2	13 941.5	15 151.6	13 298.7	11 843.7
0.808	1.535	16 096.5	14 218.2	15 375.1	13 619.3	12 312.1
0.806	1.538	16 161.0	14 266.0	15 591.3	13 938.8	12 777.5
0.804	1.542	16 462.9	14 314.4	15 832.0	14 287.2	13 223.2
0.802	1.546	16 823.9	14 617.0	16 048.7	14 670.3	13 661.5
0.800	1.550	16 861.6	14 942.4	16 134.0	15 096.0	14 098.4
0.798	1.554	16 938.0	14 999.1	16 361.9	15 145.4	14 508.5
0.796	1.558	17 298.6	15 325.1	16 598.8	15 602.5	14 922.0
0.794	1.562	17 340.5	15 387.1	16 673.5	14 094.8	15 295.7
0.792	1.566	17 382.7	15 745.1	16 903.5	16 153.6	15 678.8
0.790	1.570	17 768.2	15 779.02	17 163.0	16 207.8	16 035.3
0.788	1.574	17 819.3	15 848.1	17 391.7	16 771.7	16 372.4
0.786	1.578	18 219.9	16 210.5	17 476.9	16 816.2	16 707.1
0.784	1.582	18 276.4	16 248.5	17 718.0	16 854.8	17 021.1
0.782	1.586	18 693.1	16 325.4	17 992.3	17 500.8	17 057.7
0.780	1.590	18 755.9	16 732.4	18 230.9	17 547.0	17 401.6
0.778	1.594	18 802.1	16 775.2	18 504.6	17 593.7	17 772.6
0.776	1.598	18 854.6	16 822.9	18 791.3	17 641.0	17 815.6
0.774	1.602	19 298.5	16 862.3	19 036.5	18 391.7	18 222.1
0.772	1.606	19 350.5	17 282.4	19 120.4	18 450.0	18 283.8
0.770	1.610	19 841.1	17 331.1	19 408.9	18 489.3	18 677.3

RIGHTSLINK

Table II. (*Continued.*)

λ (μm)	Energy (eV)	Absorption coefficient vs electron concentration 1.3×10^{17} (cm^{-1})	3.7×10^{17} (cm^{-1})	1.0×10^{18} (cm^{-1})	2.2×10^{18} (cm^{-1})	3.8×10^{18} (cm^{-1})
0.768	1.615	19 885.1	17 385.4	19 712.0	18 529.1	18 729.5
0.766	1.619	19 936.9	17 840.6	19 774.4	19 437.6	19 158.1
0.764	1.623	20 465.8	17 890.6	20 063.8	19 475.7	19 210.2
0.762	1.627	20 516.3	18 387.1	20 130.1	19 488.5	19 256.9
0.760	1.632	20 567.4	18 437.5	20 197.0	19 527.2	19 719.4
0.758	1.636	21 160.9	18 482.1	20 472.5	19 566.2	19 758.4
0.756	1.640	21 200.1	19 034.8	20 543.3	19 645.5	20 261.2
0.754	1.645	21 239.6	19 078.7	20 873.0	19 685.8	20 312.4
0.752	1.649	21 279.5	19 123.1	20 910.7	20 823.9	20 848.7
0.750	1.653	21 935.3	19 152.9	21 261.5	20 860.4	20 898.4
0.748	1.658	21 981.8	19 771.5	21 549.2	20 878.7	20 948.5
0.746	1.662	22 028.8	19 814.9	21 633.9	20 934.3	20 990.8
0.744	1.667	22 757.1	19 849.9	21 940.2	20 953.0	21 596.4
0.742	1.671	22 784.9	19 876.4	22 310.5	20 990.7	21 635.2
0.740	1.676	22 826.9	20 576.4	22 310.4	21 009.7	21 664.5
0.738	1.680	22 855.2	20 607.7	22 704.7	21 048.0	21 703.7
0.736	1.685	22 883.6	20 639.3	22 704.7	22 646.1	22 370.4
0.734	1.689	23 743.8	20 692.4	23 126.5	22 675.4	22 404.6
0.732	1.694	23 901.4	21 501.9	23 126.5	22 704.9	22 439.1
0.730	1.699	23 795.7	21 540.8	23 521.2	22 704.9	22 473.8
0.728	1.703	23 830.7	21 566.9	23 579.8	22 734.6	23 228.1

centration if all the impurities were ionized with no compensation ($n_0=N_D$). The data suggest that the impurities were fully ionized with no compensation in all the films with the exception of those with $n_0=2.4\times10^{18}$ cm^{-3}, for which the actual selenium concentration deduced from SIMS was $N_{Se}\simeq4.1\times10^{18}$ cm^{-3}. The mass spectra of the two most highly doped films (these have similar selenium concentrations) reveal no other impurities that could cause compensation. Finally, Table III shows the measured mobilities of the samples. These mobilities are consistent with data previously reported for *n*-GaAs;[34,35] this includes the mobility of the sample with $n_0=2.4\times10^{18}$ cm^{-3}. We therefore see no evidence of compensation in any of these films.

SIMS measurements showed that the actual selenium concentration was $N_{Se}\simeq4.1\times10^{18}$ cm^{-3} for our reduced-growth-rate films in which $n_0=2.4\times10^{18}$ cm^{-3}, and that $N_{Se}\simeq3.7\times10^{18}$ cm^{-3} for the films with $n_0=3.8\times10^{18}$ cm^{-3}. This similarity of N_{Se} could explain the similarity in $\alpha(h\nu)$ between these two electron concentrations, which is depicted in Fig. 7. Note also that Casey and Stern estimated that $N_D^+/N_A^-=5$ for the samples used by Casey and co-workers. If they had had a sample with a free-electron concentration of $n_0\simeq2.4\times10^{18}$ cm^{-3}, the ionized impurity concentration would correspond to $N_D^++N_A^-\simeq3.6\times10^{18}$ cm^{-3}, nearly the same concentration as our $n_0=3.8\times10^{18}$ cm^{-3}. Such similarity in N_{Se} could explain why our $\alpha(h\nu)$ for $n_0=3.8\times10^{18}$ cm^{-3} is so similar to the results of Casey

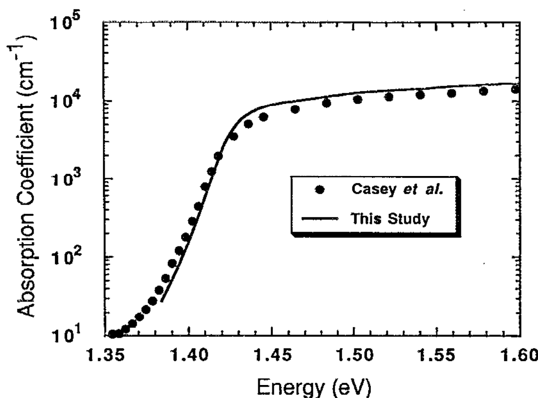

FIG. 8. Comparison of our results for $n_0=3.7\times10^{17}$ cm^{-3} to those of Casey and co-workers (Ref. 12). The "data points" of Casey and co-workers are interpolated. There is agreement at the absorption edge, but significant differences exist at photon energies greater than the band gap.

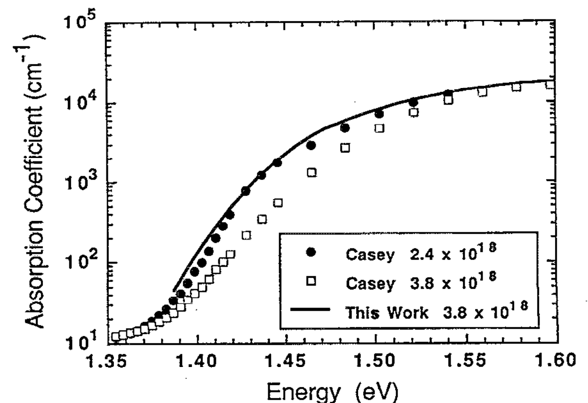

FIG. 9. Comparison of our results for $n_0=3.8\times10^{18}$ cm^{-3} to those of Casey and co-workers (Ref. 12) interpolated for $n_0=2.4$ and 3.8×10^{18} cm^{-3}.

RIGHTSLINK

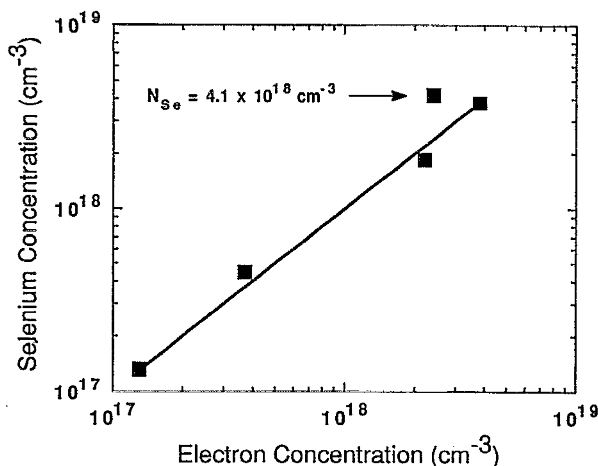

FIG. 10. Comparison of free-electron concentration and relative selenium concentration. The abscissa is the electron concentration as measured by the van der Pauw technique, the ordinate is the selenium concentration as measured by SIMS, and the line represents the expected electron concentration if all the impurities were ionized with no compensation ($n_0=N_D$). The data suggest that the impurities were fully ionized in all the films with the exception of those with $n_0=2.4\times10^{18}$ cm^{-3} for which the actual selenium concentration was $N_{Se}=4.1\times10^{18}$ cm^{-3}.

and co-workers, interpolated to $n_0=2.4\times10^{18}$ cm^{-3}. As a final comparison, we found that Casey's data interpolated to $n_0=1.5\times10^{18}$ cm^{-3}, which corresponds to $N_D^+ + N_A^- \simeq 2.2\times10^{18}$ cm^{-3}, agrees in the absorption tail with our results for $n_0=2.2\times10^{18}$ cm^{-3}. The additional impurities in Casey and co-workers' melt-grown material and ours with $n_0=2.4\times10^{18}$ cm^{-3} apparently further disturbed the density of states making comparison of results as a function of free-electron density difficult.

VI. SUMMARY AND CONCLUSIONS

We have measured the near-band-edge optical-absorption coefficient for n-type GaAs with a large range of electron concentration. For $\alpha(h\nu)<3000$ cm^{-1}, our results agree with the classic work of Casey and co-workers for $n_0<10^{18}$ cm^{-3}. For photon energies above the band-gap energy, however, our results as determined from transmission experiments are 20%–25% greater than Casey and co-workers' $\alpha(h\nu)$ which were deduced from a Kramers–Kroenig analysis. Since our $\alpha(h\nu)$ (excepting those of $n_0=3.7\times10^{17}$ cm^{-3}) approach the same value at high energies (to within $\pm3\%$ at $h\nu=1.7$ eV), and Casey and co-workers' results showed similar self-agreement ($\pm15\%$ at $h\nu=1.6$ eV), the relative differences at high energy between the studies are likely due to a systematic difference related to the two measurement techniques or to the two material growth methods.

For $n_0>10^{18}$ cm^{-3}, our results for $\alpha(h\nu)<3000$ cm^{-1} differ substantially from the results of Casey and co-workers and this difference becomes more significant with increasing electron concentration. The differences was as much as a factor of 4 for $\alpha(1.42$ eV$)$ at $n_0=3.8\times10^{18}$ cm^{-3}. The results presented here provide an accurate characterization of the concentration-dependent, near-band-edge absorption coefficient in high-quality, uncompensated, n-type GaAs. As such, they should prove useful for modeling optoelectronic devices as well as for more fundamental band-structure studies.

TABLE III. Mobility vs electron density measured by van der Pauw technique.

n_0 (cm^{-3})	Mobility (cm^2 V^{-1} s^{-1})
1.3×10^{17}	3950
3.7×10^{17}	3110
1.0×10^{18}	2500
2.2×10^{18}	1990
2.4×10^{18}	2070
3.8×10^{18}	1850

ACKNOWLEDGMENTS

The authors would like to thank R. Alferos for his assistance in growing the double heterostructures at the Varian Research Center, G. Chen for doing the mobility measurements at Purdue University, and G. Bazan for the SEM measurements at the University of Notre Dame. This work was supported by the National Renewable Energy Laboratory and by Varian Associates.

APPENDIX

Equation (2) can be modified to fit the form of[27]

$$\int_{m\pi}^{(m+1)\pi} \frac{dx}{a^2+b^2\sin^2 cx} = \left[\frac{1}{ac\sqrt{a^2+b^2}}\tan^{-1}\left(\frac{\sqrt{a^2+b^2}}{a}\tan(cx)\right)\right]_{m\pi}^{(m+1)\pi}, \quad \text{(A1)}$$

if $a=(1-R)$, $b=2\sqrt{R}$, $c=1$, and $\Theta=x$. As defined in the text, T_{ave} can then be written as

$$T_{ave}=\frac{1}{\pi}\left[\frac{1-R}{1+R}\tan^{-1}\left(\frac{1+R}{1-R}\tan\Theta\right)\right]_{m\pi}^{(m+1)\pi}. \quad \text{(A2)}$$

In Eq. (A2) $\tan\Theta=0$ for both limits of integration. The inverse tangent, however, does not necessarily represent the principal value. One should use that branch of the inverse tangent corresponding to the value of Θ employed.[27] Therefore,

$$T_{ave}=\frac{1}{\pi}\left(\frac{1-R}{1+R}\right)[(m+1)\pi-m\pi]=\left(\frac{1-R}{1+R}\right), \quad \text{(A3)}$$

and this leads to

$$R=\frac{1-T_{ave}}{1+T_{ave}}. \quad \text{(A4)}$$

[1] R. K. Ahrenkiel, B. M. Keyes, G. B. Lush, M. R. Melloch, M. S. Lundstrom, and H. F. MacMillan, J. Vac. Sci. Technol. **10**, 990 (1992).
[2] C. J. Hwang, J. Appl. Phys. **40**, 3731 (1969).

RIGHTSLINK

[3] H. B. Bebb and E. W. Williams, *Photoluminescence I: Theory in Semiconductors and Semimetals* (Academic, New York, 1972), Vol. 8, p. 219.
[4] H. C. Casey, Jr. and Frank Stern, J. Appl. Phys. **47**, 631 (1976).
[5] P. Asbeck, J. Appl. Phys. **48**, 820 (1977).
[6] R. J. Nelson and R. G. Sobers, J. Appl: Phys. **49**, 6103 (1978).
[7] R. K. Ahrenkiel, D. J. Dunlavy, B. Keyes, S. M. Vernon, T. M. Dixon, S. P. Tobin, K. L. Miller, and R. E. Hayes, Appl. Phys. Lett. **55**, 1088 (1989).
[8] T. Kuriyama, T. Kamiya, and H. Yanai, Jpn. J. Appl. Phys. **16**, 465 (1977).
[9] B. E. Sernelius, Phys. Rev. B **33**, 8582 (1986).
[10] P. E. Schmid, Phys. Rev. B **23**, 5531 (1981).
[11] A. L. Efros, Sov. Phys. Usp. **16**, 789 (1974).
[12] H. C. Casey, Jr., D. D. Sell, and K. W. Wecht, J. Appl. Phys. **46**, 250 (1975).
[13] W. van Roosbroeck and W. Shockley, Phys. Rev. **94**, 1558 (1954).
[14] D. E. Hill, Phys. Rev. **133**, A866 (1964).
[15] G. B. Lush, H. F. MacMillan, B. M. Keyes, D. H. Levi, R. K. Ahrenkiel, M. R. Melloch, and M. S. Lundstrom, J. Appl. Phys. **72**, 1436 (1992).
[16] M. Tong, D. Ballegeer, A. Ketterson, E. J. Roan, K. Y. Cheng, and I. Adesida, J. Electon. Mater. **21**, 9 (1992).
[17] M. Konagai, M. Sugimoto, and K. Takahashi, J. Cryst. Growth **45**, 277 (1978).
[18] C. Juang, K. J. Kuhn, and R. B. Darling, J. Vac. Sci. Technol. B **8**, 1122 (1990).
[19] E. Yablanovitch, T. Gmitter, J. P. Harbison, and R. Bhat, Appl. Phys. Lett. **51**, 2222 (1987).
[20] M. Born and E. Wolf, *Principles of Optics*, 6th ed. (Pergamon, New York, 1980).
[21] O. S. Heavens, *Optical Properties of Thin Solid Films* (Academic, New York, 1955).
[22] D. E. Aspnes, S. M. Kelso, R. A. Logan, and R. Bhat, J. Appl. Phys. **60**, 754 (1986).
[23] H. C. Casey, Jr., D. D. Sell, and M. B. Panish, Appl. Phys. Lett. **24**, 63 (1974).
[24] D. D. Sell, H. C. Casey, Jr., and K. W. Wecht, J. Appl. Phys. **45**, 2650 (1974).
[25] D. D. Sell and H. C. Casey, Jr., J. Appl. Phys. **45**, 800 (1974).
[26] H. A. Haus, *Waves and Fields in Optoelectronics* (Prentice-Hall, Englewood Cliffs, NJ, 1984), p. 65.
[27] W. H. Beyer, *CRC Standard Mathematical Tables*, 28th ed. (CRC, Boca Raton, FL, 1987), p. 268.
[28] F. Urbach, Phys. Rev. **92**, 1324 (1953).
[29] J. S. Blakemore, J. Appl. Phys. **53**, R149 (1982).
[30] J. I. Pankove, Phys. Rev. **140**, A2059 (1965).
[31] E. Burstein, Phys. Rev. **93**, 632 (1954).
[32] F. Stern, *Solid State Physics*, edited by F. Seitz and D. Turnbull (Academic, New York, 1963), Vol. 15, p. 300.
[33] M. D. Sturge, Phys. Rev. **127**, 768 (1962).
[34] D. A. Anderson, N. Apsley, P. Davies, and P. L. Giles, J. Appl. Phys. **58**, 3059 (1985).
[35] D. M. Szmyd, M. C. Hanna, and A. Majerfeld, J. Appl. Phys. **68**, 2376 (1990).

RIGHTSLINK